Relaxation oscillations and negative strain rate sensitivity in the Portevin–Le Chatelier effect

S. Rajesh[1] and G. Ananthakrishna[1,2,*]
[1]*Materials Research Center, Indian Institute of Science, Bangalore 560 012, India*
[2]*Center for Condensed Matter Theory, Indian Institute of Science, Bangalore 560 012, India*
(Received 30 November 1998; revised manuscript received 22 November 1999)

A characteristic feature of the Portevin–Le Chatelier effect, or the jerky flow, is the stick-slip nature of stress-strain curves which is believed to result from the negative strain rate dependence of the flow stress. The latter is assumed to result from the competition of a few relevant time scales controlling the dynamics of jerky flow. We address the issue of time scales and its connection to the negative strain rate sensitivity of the flow stress within the framework of a model for the jerky flow, which is known to reproduce several experimentally observed features, including the negative strain rate sensitivity of the flow stress. We attempt to understand the above issues by analyzing the geometry of the slow manifold underlying the relaxational oscillations in the model. We show that the nature of the relaxational oscillations is a result of the atypical bent geometry of the slow manifold. The analysis of the slow manifold structure helps us to understand the time scales operating in different regions of the slow manifold. Using this information we are able to establish connection with the strain rate sensitivity of the flow stress. The analysis also helps us to provide a proper dynamical interpretation for the negative branch of the strain rate sensitivity.

PACS number(s): 05.45.−a, 83.50.By

I. INTRODUCTION

The Portevin–Le Chatelier effect [1], or the jerky flow, has been an object of continued interest in materials science for quite some time. The phenomenon refers to an instability seen in the form of repeated stress drops followed by periods of reloading observed when tensile specimens are deformed in a certain range of strain rates and temperatures [2]. The effect is seen in many interstitial and substitutional metallic alloys (commercial aluminum, brass, alloys of aluminum and magnesium [3], etc.). Each of the load drops is related to the formation and propagation of dislocation bands [3,4]. The traditional picture of the instability is that it stems from dynamic interaction of mobile dislocations with solute atoms and is called dynamic strain ageing [2]. It is this that is expected to lead to negative strain rate sensitivity (SRS) of the flow stress [3–7].

Plastic flow is intrinsically nonlinear and therefore methods of nonlinear dynamics have a natural role to play in understanding plastic instabilities [4,8–11]. Use of these new techniques have led to insights which were hitherto not possible. The first attempt to look at the phenomenon from a nonlinear dynamical angle was taken by Ananthakrishna and co-workers [8], which offers a natural basis for the description of the time dependent aspects of the Portevin–Le Chatelier (PLC) effect which were ignored in the earlier theories [5–7]. Their model allows for explicit inclusion and interplay of different time scales inherent in the dynamics of dislocations. These authors show that the occurrence of the instability is a consequence of Hopf bifurcation as a function of the applied strain rate. Many known features of the PLC effect such as the existence of a window of strain rates and temperatures within which it occurs, etc., were correctly reproduced. Most importantly, and for the first time, the negative SRS was shown to emerge naturally in the model, as a result of nonlinear interaction of the participating defects. It also predicts the existence of chaotic stress drops in a range of strain rates, which has been recently verified [12–15]. Even the number of degrees of freedom estimated turn out to be the same as in the model offering justification for ignoring spatial degrees of freedom (see Ref. [16] also). Further dynamical analysis of the model for the creep case has shown that the temperature dependence of the strain bursts is consistent with experimental findings [17,18].

The study of the PLC effect from a dynamical angle has been useful in elucidating several features; but it has also brought certain other issues into sharp focus which were hitherto not investigated in depth. This paper is intended to address one such issue related to the time scales relevant to the dynamics of the PLC effect within the framework of the above model. This is reflected in the two well known attributes of the PLC effect, namely, the negative strain rate behavior of the flow stress and the stick-slip or relaxational nature of the dynamics reflected in the stress time series. In order to motivate, we will present arguments showing that conflicting conclusions can be arrived at when one analyzes this question starting from these two angles.

We start with a discussion of the well accepted physical picture of the PLC effect, namely, dynamic strain ageing. At a qualitative level, theories of strain ageing already have an implicit suggestion that the occurrence of the negative SRS is related to the competition of diffusive time scale and the waiting time of dislocations at obstacles [5,6], even though there is no dynamics involved in these theories. The physical picture of strain ageing is as follows. At small velocities, solute atoms have enough time to diffuse to the temporarily arrested dislocations thus providing additional pinning thereby impeding their breakaway from localized obstacles. Due to the constant applied strain rate, the overall stress to keep the dislocations moving increases bringing the stress to a threshold level beyond which dislocations break away

*Electronic address: garani@mrc.iisc.ernet.in

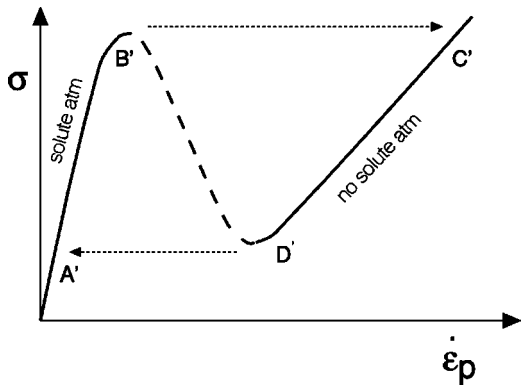

FIG. 1. Schematic plot of the SRS. Branch $B'D'$ shown by the dashed line describes the negative strain rate sensitivity of the PLC effect. Dotted lines represent the discontinuous strain rate jumps leading to serrations in the stress-strain curve.

[5,6]. At high velocities, such additional pinning due to solute atoms is not possible since the waiting time of dislocations at obstacles is too short for the diffusion to occur. A schematic diagram of the SRS is shown in Fig. 1. In the language of the stick-slip dynamics, the branch $A'B'$ corresponds to the stick state and $B'C'$ to the slip state (Fig. 1). The slope of stress verses velocity (''friction coefficient'') at low velocities is much higher than that corresponding to high velocities since in the former case, solute atoms have to be dragged along with the dislocations, while in the latter case there is no solute atmosphere. Based on physical considerations, these two stable branches are *assumed* to be separated by *an unstable* branch with a negative slope to reflect the nonaccessible nature.

The occurrence of the negative flow rate characteristic is not just limited to the PLC effect [19,20]. With particular reference to the conceptual aspects of the negative branch, we cite two other mechanical systems, namely, the peeling of an adhesive tape and frictional sliding of a block of material over another [19,20] which shows the inaccessible nature of the negative slope branch. However, in the case of the PLC effect, there have been attempts to obtain experimental points in this domain of strain rates [21,22] which has led to some confusion about the measurability of the negative slope branch of the SRS which will be discussed later (Sec. V). Therefore, it is important to understand the meaning of the negative branch of SRS from a dynamical point of view with reference to the PLC effect which hopefully will lead to a better understanding of other stick-slip phenomenon.

Returning to the PLC effect, Penning [23] was the first to recognize that the negative SRS could be used to explain the strain rate jumps observed in experiments. Subsequently, the negative SRS feature has been used as an input into several theories [24,25]. In particular, it has helped to successfully explain the nature of yield drops occurring in different regimes of strain rate and temperature [25]. Pertinent to our discussion of time scales inherent to the PLC effect, we note that in such theories, *two slow time scales* corresponding to the two dissipative branches, $A'B'$ and $C'D'$, show up along with *two fast time scales* corresponding to the jumps ($B'C'$ and $D'A'$) in the strain rates. A more direct reflection of the time scales inherent to the dynamics of the PLC effect can be deduced from stress-strain curve.

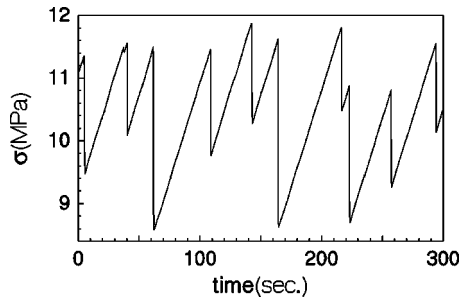

FIG. 2. Stress-time plot for single crystal of $Cu-10\%$ Al deformed at constant strain rate of $\dot{\epsilon}=3.3\times10^{-6}$ s^{-1}.

To facilitate discussion of time scales involved in an experimental stress-time series, consider the so called machine equation written as

$$\dot{\sigma}_a=\kappa[\dot{\epsilon}_a-\dot{\epsilon}_p], \tag{1}$$

where σ_a, $\dot{\epsilon}_a$, and $\dot{\epsilon}_p$ refer to the stress, applied strain rate, and plastic strain rate, respectively, and κ is the combined elastic constant of the machine and the sample. We note that only stress is monitored by the load sensing device. Apart from this, it is possible to measure the plastic strain rate using strain gauges or using cinematographic techniques [26]. Using Eq. (1), we can now identify different time scales in an experimental curve. Consider a typical stress-strain curve for an applied strain rate of 8.3×10^{-5} s^{-1} for the PLC effect in $Cu-10\%$ Al is shown in Fig. 2. (For our purpose, we will ignore the nonperiodic nature.) From the sawtooth shape of the stress-strain series, two points emerge: (a) the positive slope of $\sigma_a-\epsilon_a$ curve is close to the elastic loading rate ($\kappa\dot{\epsilon}_a$), and (b) the duration of each stress drop is very short. From Eq. (1), we see that the stress drop duration is the time interval during which $\dot{\epsilon}_p(t)$ larger than $\dot{\epsilon}_a$. We also note that the changes in slopes, when they occur, are abrupt (within the recording accuracy of 0.05 s^{-1}). Knowing that $\dot{\epsilon}_p$ is proportional to the mobile dislocation density and using Eq. (1), we can see that the mobile dislocation density should be nearly constant in the rising part of σ-ϵ_a curve and therefore correspond to the stick state. Further, the short duration of the stress drop should be a result of rapid multiplication of mobile dislocation and therefore corresponds to the slip state. This must be followed by the process of immobilization of dislocations. However, the abrupt change in the slope (from negative to positive) also implies that the immobilization time scale is also fast. Indeed, as is clear from Fig. 2, it is not possible to separate out these two fast time scales. Thus, from the stress-strain curve, we see only *one slow time scale* and *two fast time scales* which is in apparent conflict with what was argued from the schematic diagram of the orbit $A'B'C'D'$ in Fig. 1. This discussion raises several questions relating to the origin of these time scales causing jumps in dislocation densities which needs to be understood if the above inconsistency has to be resolved. Specifically, (i) What is the dynamical mechanism which keeps the mobile dislocation density constant and in low levels for long intervals of time? (ii) What are the mechanisms for rapid multiplication and immobilization of mobile dislocations? As we shall see, resolving these issues will also

help us to interpret the negative SRS in an appropriate way. Further, associating various time scales with different branches of the SRS provides a better insight into the stick-slip dynamics of the PLC effect.

Analysis of time scales can be best understood from a dynamical point of view. It is well known that relaxation oscillations are at the root of stick-slip behavior. One of the standard ways of understanding relaxation oscillations is by analyzing the slow manifold geometry [27–31] of the underlying model. Following this, we shall attempt to understand the above issues from the point of view of relaxation oscillations. The paper is organized as follows. In Sec. II, we briefly introduce the model along with the known results. In Sec. III, we state some bifurcation features relevant for further discussion. In Sec. IV, we show that the nature of relaxation oscillation in the model is *atypical* and is due to the bent nature of the slow manifold of the model. This analysis further helps us to understand the dynamical basis of different time scales relevant to the PLC effect. In Sec. V, we discuss the concept of negative SRS and its measurement in some detail to highlight the meaning of the negative branch. Using the geometry of the slow manifold, we calculate the dependence of stress on the plastic strain rate and show the connection between the various branches of the SRS and the time scales operating in different regions of slow manifold which in turn helps us to resolve the inconsistency of time scales. Section VI is devoted to discussion and conclusions.

II. DYNAMICAL MODEL FOR JERKY FLOW

The model consists of mobile dislocations and immobile dislocations and another type which mimics Cottrell's type, which are dislocations with clouds of solute atoms [8]. Let the corresponding densities be N_m, N_{im}, and N_i, respectively. The rate equations for the densities of dislocations are

$$\dot{N}_m = \theta V_m N_m - \beta N_m^2 - \beta N_m N_{im} + \gamma N_{im} - \alpha_m N_m, \quad (2)$$

$$\dot{N}_{im} = \beta N_m^2 - \beta N_{im} N_m - \gamma N_{im} + \alpha_i N_i, \quad (3)$$

$$\dot{N}_i = \alpha_m N_m - \alpha_i N_i. \quad (4)$$

The overdot, here, refers to the time derivative. The first term in Eq. (2) is the rate of production of dislocations due to cross glide with a rate constant θ. V_m is the velocity of the mobile dislocations which in general depends on some power of the applied stress σ_a. The second term refers to the annihilation or immobilization of two mobile dislocations. The third term also represents the annihilation of a mobile dislocation with an immobile one. The fourth term represents the remobilization of the immobile dislocations due to stress or thermal activation [see γN_{im} in Eq. (3)]. The last term represents the immobilization of mobile dislocations either due to solute atoms or due to other pinning centers. α_m refers to the concentration of the solute atoms which participate in slowing down the mobile dislocations. Once a mobile dislocation starts acquiring solute atoms we regard it as a new type of dislocation, namely, Cottrell's type N_i, i.e, the incoming term in Eq. (4). As they acquire more and more solute atoms they slow down and eventually stop the dislocation entirely. At this point, they are considered to have transformed to N_{im} [loss term in Eq. (4) and a gain term in Eq. (3)]. Indeed, the whole process can be mathematically represented by defining $N_i = \int_{-\infty}^{t} K(t-t') N_m(t') dt' = \alpha_m \int_{-\infty}^{t} \exp[-\alpha_i (t-t')] N_m(t') dt'$, which represents the entire process of slowing down of N_m in an exponential fashion with a time constant α_i. (The choice of K as having an exponential form is obviously a simplification of the actual process.)

These equations should be dynamically coupled to the machine equation which now takes the form

$$\dot{\sigma}_a = \kappa(\dot{\epsilon}_a - B_0 N_m V_m), \quad (5)$$

where V_m is the velocity of mobile dislocations and B_0 is the Burgers vector. A power law dependence of $V_m = V_0 (\sigma_a / \sigma_0)^m$ is used. These equations can be cast into a dimensionless form by using scaled variables $x = N_m(\beta/\gamma)$, $y = N_{im}(\beta/\theta V_0)$, $z = N_i(\beta\alpha_i/\gamma\alpha_m)$, $\tau = \theta V_0 t$, and $\phi = \sigma_a/\sigma_0$:

$$\dot{x} = \phi^m x - a x - b_0 x^2 - xy + y, \quad (6)$$

$$\dot{y} = b_0 (b_0 x^2 - xy - y + az), \quad (7)$$

$$\dot{z} = c(x - z), \quad (8)$$

$$\dot{\phi} = d(e - \phi^m x). \quad (9)$$

Here $a = \alpha_m/\theta V_0$, $b_0 = \gamma/\theta V_0$, $c = \alpha_i/\theta V_0$, $\kappa = (\theta\beta\sigma_0 d/\gamma B_0)$, and $e = (\dot{\epsilon}_a \beta / B_0 V_0 \gamma)$. For these sets of equations there is only one steady state which is stable. There is a range of the parameters a, b, c, d, m, and e for which the linearized equations are unstable. In this range x, y, z, and ϕ are oscillatory.

Among these physically relevant parameters, we study the behavior of the model as a function of the most important parameters, namely, the applied strain rate e and the velocity exponent m. The values of other parameters are kept fixed at $a = 0.7$, $b_0 = 0.002$, $c = 0.008$, and $d = 0.0001$. As can be verified, these equations exhibit a strong volume contraction in the four-dimensional phase space. We note that there are widely differing time scales corresponding to a, b_0, c, and d (in decreasing order) in the dynamics of the model. For this reason, the equations are stiff and the numerical integration routines were designed specifically to solve this set of equations. We have used a variable order Taylor series expansion method as the basic integration technique where the coefficients are determined using a recursive algorithm.

III. SUMMARY OF BIFURCATION EXHIBITED THE MODEL

The model exhibits a rich variety of dynamics such as period bubbling, period doubling, and complex bifurcation sequences referred to as mixed mode oscillations in literature. Here, we will briefly recall only those aspects of the bifurcation diagram relevant for the discussion of relaxation oscillations. The gross features of the phase diagram in the (m,e) plane are shown in Fig. 3. In our discussion, we use e as the primary control parameter and m as the unfolding

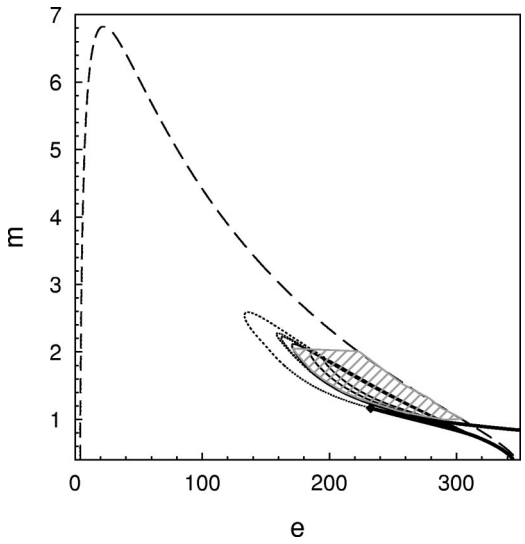

FIG. 3. Phase diagram of the model in (m,e) plane. See text for details. The broken line corresponds to the locus of Hopf bifurcations and the dotted lines to the successive period doubling bifurcations. See text for details.

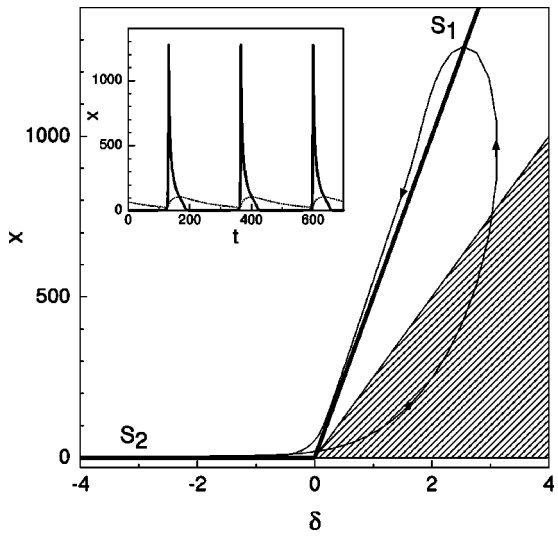

FIG. 4. Evolution of a trajectory (thin lines) along with the bent-slow manifold (S_1 and S_2 shown by thick lines) structure in the x-δ plane, for $m=1.2$ and $e=200$. Inset shows the time series of the x variable (continuous line) and z variable (dotted line).

parameter. For values of $m>m_d\sim 6.8$, the equilibrium fixed point of the system of equations, denoted by (x_0,y_0,z_0,ϕ_0), is stable. Both x_0 and z_0 are $\sim e/2$ and y_0 and ϕ_0 are independent of e. At $m=m_d$, we have a degenerate Hopf bifurcation as a function of e. For values less than m_d, we have a back-to-back Hopf bifurcation, the first occurring at $e=e_{c_1}$ and the reverse at $e=e_{c_2}$. The periodic orbit connecting these back-to-back Hopf bifurcations is referred to as the principal periodic orbit. The dynamics of the system is essentially bounded by these two Hopf bifurcations. In Fig. 3, the broken line represents the Hopf bifurcation and the dotted lines correspond to the locus of the first three successive period doubling bifurcations. The inner, continuous lines represent the locus of saddle node bifurcations corresponding to periods 3, 4, and 5 which are the first three dominant periodic windows in the alternating periodic chaotic bifurcation sequence. Complex bifurcation sequences, characterized by alternate periodic-chaotic sequences are seen in the hatched region of the parameter space. A codimension two bifurcation points in the form of a cusp at (e_c,m_c) formed by the merging of the locus of two saddle node bifurcations of the principal periodic orbit (represented by bold lines) is shown as a filled diamond in Fig. 3. Bifurcation diagrams have been obtained by plotting the maxima of any one of the variables x, y, z or ϕ as a function of the control parameters (e,m).

IV. MECHANISM OF RELAXATION OSCILLATIONS

One characteristic feature of the dynamics of the system is its strong relaxational nature. This feature persists even in regions of the (m,e) plane wherein complex periodic-chaotic oscillations are seen (hatched region in Fig. 3). The presence of relaxations oscillations and complex periodic chaotic oscillations are interrelated and are a result of the geometry of the slow manifold. (For details see Ref. [32].) Relaxation oscillations that manifest in the model are a type of relaxation oscillation wherein the fast variable takes on large values for a short time after which it assumes small values of the same order of magnitude as that of the slow variables. The time spent by the fast variable in the part of phase space where the amplitude is small is a substantial portion of the period of the orbit. Typical plots of $x(t)$ (continuous line) and $z(t)$ (dotted line) are shown in the inset of Fig. 4 for $e=200.0$ and $m=1.2$.

To understand the nature of the relaxation oscillations, we first study the structure of the slow manifold (S) and the behavior of the trajectories visiting different regions of S. The slow manifold of a multiple time scale dynamical system is given by the surface spanning the time invariant solutions of the fast variable. In our case, it is given by

$$\dot{x}=g(x,y,\phi)=-b_0x^2+x\delta+y=0 \tag{10}$$

with $\delta=\phi^m-y-a$. Here, the slow variables y and ϕ (and therefore δ) are regarded as parameters. Further, as we will see below, it is simpler to deal with the structure of the slow manifold in terms of the δ instead of both y and ϕ. Then, the physically allowed solution of the above equation is

$$x=\frac{\delta+\sqrt{\delta^2+4b_0y}}{2b_0}, \tag{11}$$

where δ can take on both positive and negative values. Noting that b_0 is small and therefore $\delta^2\gg 4b_0y$, two distinct cases arise corresponding to $\delta>0$ and $\delta<0$ for which $x\sim\delta/b_0$ and $x\sim -y/\delta$, respectively. Further, since the slow variable ϕ and y take on values of the order of unity, the range of $\delta=\delta(y,\phi)$ is of the same order as that of ϕ and y (as is evident from Figs. 4 and 5). Thus, we see that $x\sim -y/\delta$ is small and $x\sim\delta/b_0$ is large. For values around $\delta=0$ and positive, we get $x\sim(y/b_0)^{1/2}$.

The bent-slow manifold structure along with the two portions of the slow manifold, namely, S_1 $(\delta>0)$ and S_2 $(\delta<0)$ are shown by bold lines in the (x,δ) plane in Fig. 4. We have also shown a trajectory corresponding to a monoperi-

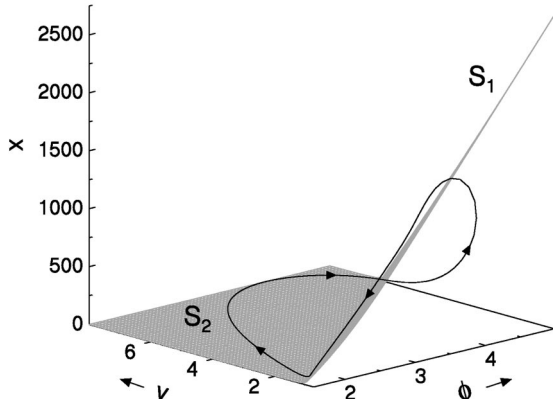

FIG. 5. Evolution of the trajectory along with the bent-slow manifold (S_1 and S_2) structure in (x,y,ϕ) space indicated by the gray plane, for $m=1.2$ and $e=200.0$.

odic relaxation oscillation ($m=1.2$ and $e=200.0$) by a thin line. As can be seen, the trajectory spends most of the time on S_1 and S_2. A local stability analysis for points on S_1 and S_2 shows that $\partial g/\partial x=\delta-2b_0x$ is negative implying that the rate of growth of x is damped. Hence these regions, S_1 and S_2 will be referred to as attracting or ''stable.'' For points below the line $2b_0x=\delta$ ($\delta>0$), $\partial g/\partial x>0$ and hence we call this region as ''unstable'' (shaded region of Fig. 4). Even then, the trajectory starting on S_2 does continue in the direction of increasing δ beyond $\delta=0$. We note that this region is not a part of the slow manifold. Once the trajectory is in this region, it moves up rapidly in the x direction (due to the ''unstable'' nature) until it reaches $x=\delta/2b_0$ line, thereafter, the trajectory quickly settles down on to the S_1 part of the slow manifold as $\partial g/\partial x$ becomes negative. As the trajectory descends on S_1 approaching S_2, we see that the trajectory deviates away from S_1. This happens when the value of x is such that $2b_0x<\delta$, i.e., $\partial g/\partial x>0$. Thus, points on S_1 satisfying this condition are locally unstable. Thus, the trajectory makes a jump from S_1 to S_2 in a short time. This roughly explains the origin of the relaxation oscillation in terms of the reduced variables δ and x.

The actual dynamics is in a higher dimensional space and a proper understanding will involve analysis of the movement of the trajectory in the appropriate space. Moreover, unlike the standard S-shaped manifold with upper and lower attracting pleats with the repulsive (unstable) branch [33], in our model, both branches of the bent-slow manifold are connected, and there is no repulsive branch of the slow manifold. Thus, *the mechanism of jumping of the orbit from S_2 to S_1 is not clear*. In order to understand this, consider a three dimensional plot of the trajectory shown in Fig. 5. The region S_2 corresponding to small values of x lies more or less on the y-ϕ plane and the region S_1 corresponding to large values of x is nearly normal to the y-ϕ plane due to the large b_0^{-1} factor. Regions S_1 and S_2 are demarcated by the ''fold curve'' given by $\delta=\phi^m-y-a=0$ which dominantly lies in the y-ϕ plane. The rapidly growing nature of the trajectory lying to right of the ''fold curve'' is due to $\partial g/\partial x>0$.

The principal features of the relaxation oscillations that we need to explain are (a) the very slow time scale for evolution on S_2, (b) fast transition from S_2 to S_1, and (c) evolution on S_1. In order to understand this, it is necessary to establish how the trajectory (viz., x, y, z, and ϕ) visits various regions of the slow manifold in a sequential way. However, our emphasis is more on those aspects of relaxation oscillation pertaining to the issue of time scales raised in the Introduction, i.e., the time scales involved in the stress-time curve (Fig. 1). (A detailed investigation on the behavior of trajectories on this slow manifold has also been carried out. See Ref. [32].) However, to understand the dependence of stress $\phi(t)$, we would also require information of y which in turn depends on z. In order to understand this, we shall analyze Eqs. (7) and (9) by recasting them in terms of δ in various regions of S. This will help to understand the general features of the flow, viz., on S_2, just outside S_2 and on S_1. In the whole analysis, it would be helpful to keep in mind the range of values of x, y, z, and ϕ, shown in Figs. 4 and 5, in particular their values as the trajectory enters and leaves S_1.

First, consider rewriting Eq. (7) valid on the slow manifold S in terms of δ:

$$\dot{y}=b_0(x\delta-xy+az). \tag{12}$$

The presence of the z variable in Eq. (12) poses some problems. Using detailed arguments based on the knowledge of the magnitude of x and z just inside, on, and outside S_2, it can be shown that the trajectory enters S_2 at small values of y and leaves S_2 at relatively larger values. Further one can show that there is a turning point for y on S_2 (see Fig. 5). For details, see Ref. [32].

With this information on the evolution of y on S_2, we now consider the changes in ϕ as the trajectory enters and leaves S_2. From Eq. (9), it is clear that a yield drop starts when x is large (i.e., when $x\sim\delta/b_0$ on S_1) and ends when x is close to minimum, when the trajectory is on S_2, which implies that ϕ is small when the trajectory enters S_2. Using the value of $x=y/|\delta|$ on S_2 in Eq. (9), we find that $e\gg\phi^m y/|\delta|$, since y is near its minimum value as the trajectory enters S_2. Thus, ϕ increases linearly from small values of ϕ at a rate close to $de\ll 1$. We recall that the loading rate in the experimental stress-strain curve was $\kappa\dot{\epsilon}_a$(de in scaled variables), which now can be understood as due to the structure of the slow manifold. This is a direct consequence of the fact that the magnitude of x remains constant as $\dot{x}\sim 0$ for the entire interval the trajectory on S_2. This is consistent with what we argued from the stress-time plot (Fig. 2), namely, the mobile dislocation density should be constant during the loading period. As the trajectory moves into S_2, y goes through a maximum whereas ϕ continues to increase since $x\sim y/|\delta|$ remains small. However, as the trajectory is just outside S_2 for which $x\sim(y/b_0)^{1/2}$ for $\delta>0$ and small, $\phi^m(y/b_0)^{1/2}\sim e$, since ϕ and y are relatively large which implies that ϕ is about to decrease. The above discussion on $\dot{y}$ and $\dot{\phi}$ for region just outside and inside the fold curve also gives us the direction of movement of the trajectory in this region, namely, it enters S_2 in the region corresponding to small values of y and ϕ, and makes an exit for relatively larger values of ϕ and y (compared to their values as the trajectory enters S_2). Further, as $\dot{x}\sim 0$, we see that the dynamics on S_2 is controlled by the slow variables.

Finally, just to the right of $\delta=0$ line, $\dot{x}\sim x\delta$, with δ very small, which suggests that the time constant is small. Thus,

the growth of x is slow in the neighborhood of $\delta=0$, and is tangential to the S_2 plane even in the ''unstable'' region. However, once the trajectory moves away from $\delta=0$, the growth of the trajectory is controlled by $\partial g/\partial x$ and hence the time scale of growth of x is of the order of δ^{-1} which is of the order of unity explaining the short time span of the stress drop seen in Fig. 2. This also explains why the trajectory tends to leave stable portion of the slow manifold S_2 and move into the ''unstable'' region.

Once in the unstable region, the value of x continues to grow in this region of the phase space as can be seen from Eq. (9) until the value of x is such that $\phi^m x=e$ is satisfied. Beyond this value of ϕ, $\dot{\phi}$ is negative. Thus, the trajectory leaving S_2 eventually falls onto the S_1 part of the slow manifold. We can again evaluate $\dot{y}$ and $\dot{\phi}$ just as the trajectory reaches S_1. Using $x\sim\delta/b_0$ in Eq. (7), it can be shown that y decreases. Now, consider the equation for ϕ. Using $x\sim\delta/b_0$ on S_1, we see that $\phi^m\delta/b_0>e$. Thus $\dot{\phi}<0$ when the trajectory reaches S_1 with a time constant $\sim d/b_0$, which is relatively fast. (These statements are true only as the trajectory hits S_1.) We recall here that in the experimental time series, the stress drops from a peak value to its minimum in a very short time span. Further, we have argued that this should be the sum of contributions arising from fast multiplication of dislocations (which we have already argued has a time scale of δ^{-1}) and subsequent immobilization. The latter is reflected in another rapid time scale $\sim d/b_0$. This explains the difficulty in separating the contributions arising from the two processes in the experimental time series. Moreover, since x is a fast variable, the changes in the x component dominates the descent of the trajectory. Finally, as the trajectory approaches S_2, $\partial g/\partial x$ becomes positive and the trajectory jumps from S_1 to S_2. Combining these results, we see that the trajectory moves towards the region of smaller values of y and ϕ entering S_2 in a region of small values of y and ϕ.

In summary, the sequential way the orbit visits various parts of the phase space is as follows. The trajectory enters S_2 part of the slow manifold in regions of small y and ϕ making an exit along S_2 for relatively large ϕ and y. Thereafter, the trajectory moves through the unstable part of the phase space before falling onto the S_1 and quickly descends on S_1. This completes the cyclic movement of the trajectory and explains the geometrical feature of the trajectory shuttling between these two parts of the manifold and the associated time scales.

Now, the question that remains to be answered is, do the trajectories always visit both S_1 and S_2 or is there a possibility that the trajectory remains confined to S_1? It is clear that if the former is true, relaxation oscillations with large amplitude will occur and if the latter is true, these are likely to be nearly sinusoidal small amplitude oscillations. Here, we recall that the coordinates of the saddle focus fixed point are $x_0=z_0\sim e/2$ which is much larger than the value of $x\sim y/|\delta|$ on S_2. Thus, the fixed point located on the S_1 will be close to the ''fold'' at the first Hopf bifurcation which occurs at small values of $e=e_{c_1}\sim 5$. Due to the unstable nature of the fixed point, the trajectories spiralling out are forced onto the S_2 part of the manifold resulting in relaxation oscillation. This point has been illustrated by considering the example of

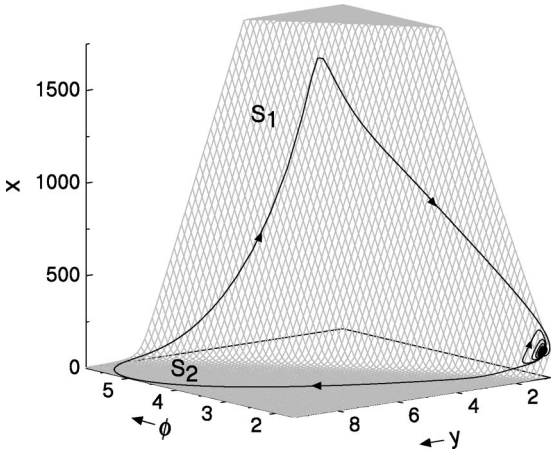

FIG. 6. Evolution of the trajectory along the bent-slow manifold (S_1 and S_2) structure for $m=1.2$ and $e=267.0$.

a period eleven orbit for $m=1.2$ and $e=267.0$ shown in Fig. 6. As is clear from this diagram, the small amplitude oscillations are located on the S_1. As e is further varied, the small amplitude oscillations grow with e, but the relaxation nature does not manifest until the orbit crosses over to S_2. To the best of the authors' knowledge the mechanism suggested here for pulsed type relaxation oscillations is new.

As we will see, the analysis of the slow manifold and the time scales operating in different parts of the phase space will be useful in providing an appropriate interpretation of the various branches of the SRS.

V. NEGATIVE STRAIN RATE SENSITIVITY

At the outset, we stress that it has been recognized that the negative unstable branch is not accessible to the dynamics of the PLC effect. Even so, early formulations and the way experimental measurements have been carried out has given rise to considerable confusion. The purpose of the material presented below is to briefly discuss the concept of negative SRS and working methods adopted in the literature, and also to clear some misconceptions.

Theories of dynamic strain ageing assume that the interaction of dislocations with solute atoms when averaged over the specimen dimensions can be represented by a constitutive relation connecting stress, strain, and strain rate which is conventionally written as [34]

$$\sigma=h\epsilon+F(\dot{\epsilon}). \tag{13}$$

The basic assumption inherent in Eq. (13) is that stress can be split into a function of ϵ and another of $\dot{\epsilon}$ alone. Then, the SRS is defined as

$$\mathcal{S}=\left.\frac{\partial\sigma}{\partial ln\dot{\epsilon}}\right|_{\epsilon}=\dot{\epsilon}\frac{d\sigma}{d\dot{\epsilon}}. \tag{14}$$

Clearly, this definition uses ϵ as a state variable. This unfortunately is not correct since strain is history dependent. In spite of this, conventionally, strain is fixed at a small nominal value and the flow stress at that value is used to obtain the SRS. It is interesting to note that the existence of critical strain for the onset of the PLC effect implies that when the

nominal strain value is lower than ϵ_c, there are no serrations even when the applied strain rate value is in the domain of the PLC effect ($e_{c_1} < e < e_{c_2}$). Yet, the onset of serrations for higher strains is somehow reflected in the measured nonmonotonic behavior of the flow stress [21]. In experiments, by fixing ϵ at some nominal value less than ϵ_c, the flow stress (at the fixed strain) is found to increase as a function of applied strain rate e for $e < e_{c_1}$, shows a decreasing trend for $e_{c_1} < e < e_{c_2}$, and again reverts to an increasing trend for $e > e_{c_2}$ [21]. Thus, the flow stress has the form shown in Fig. 1. No explanation has been offered in the literature as to why this nonmonotonic behavior should be seen. However, explanation from the dynamical point of view is fairly straightforward and is as follows. We recall here that the model predicts the existence of the critical strain ϵ_c, and also the existence of a window of strain rates $e_{c1} < e < e_{c2}$ within which serration can occur. Thus, from Eq. (9) it is easy to understand the increasing order in which the stress-strain curves are placed for increasing values of e when $e < e_{c_1}$ and $e > e_{c_2}$. In this range of e, the fixed point is stable and thus all trajectories converge to the fixed point. However, for $e_{c_1} < e < e_{c_2}$, we note that serrations result only for large enough strains, i.e., once the time of deformation is such that strain crosses ϵ_c. In our theory, serrations are equated with the existence of periodic (or aperiodic) solutions when $e_{c_1} < e < e_{c_2}$. These steady state solutions are usually reached only after transients die down. Thus, low value of nominal strain implies *short evolution time* which in turn implies that the *stress is being monitored at a transient state*. Thus, the decreasing trend of the flow stress for $e_{c_1} < e < e_{c_2}$ is a reflection of the impending periodic (aperiodic) steady state that will be reached eventually. Indeed, this was the method followed in our earlier calculation since the procedure was easy to implement numerically [8]. However, in many experimental situations, it is not possible to choose a nominal strain value low enough that it is less than ϵ_c for the entire range of strain rate values. In such a case, since the stress-strain curves are serrated, there is an ambiguity in the value of stress to be used. A working method adopted is to use a stress value as the mean value of the upper and lower stress values [22]. Then, the flow stress appears to decrease for the domain of applied strain rate values where the PLC effect manifests. Thus, this method gives the impression of actually measuring the unstable branch.

The above methods are not suitable for adoption since they do not permit the use of the knowledge of the slow manifold. There is an alternate method which uses the relaxation oscillations inherent to the dynamics of the PLC effect. In this method, by analogy with electrical analogs, one assumes that there exists a family of curves $F(\dot{\epsilon}_p)$ for each ϵ of the form shown in Fig. 1 which triggers relaxation oscillations in the form of plastic strain rate bursts and stress drops. By comparing the measured stress drops and strain bursts, one concludes the existence of the unstable branch, but one never records any points in this region. This method is suitable for our study since we will use relaxation oscillations arising in the model.

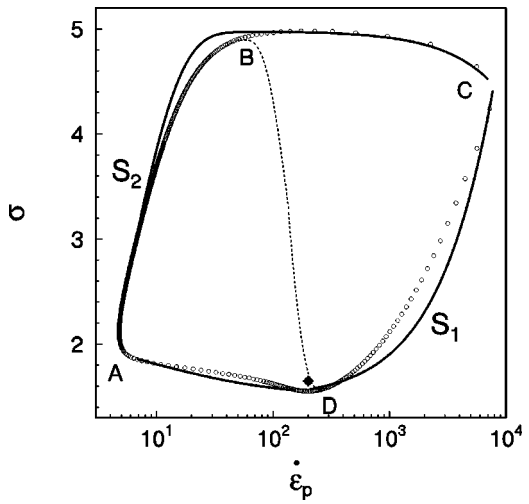

FIG. 7. Empty circles show the phase space projection of σ vs $\dot{\epsilon}_p$ corresponding to a relaxation oscillation. The unstable fixed point is shown by a filled diamond. The dotted line through the fixed point represents the apparent negative SRS region. The thick lines are analytical approximations of corresponding regions.

In the following we shall argue that the two slow time scales in the dynamics actually translate into the two stable dissipative branches of the SRS and the two fast time scales to jumps in plastic strain rate across the stable branches of the negative SRS. Since SRS represents ϕ as a function of the plastic strain rate $\dot{\epsilon}_p = \phi^m x$, in Fig. 7, we have shown a projection of the phase space trajectory on the σ-$\dot{\epsilon}_p$ plane (instead of ϕ-x) corresponding to a monoperiodic relaxation oscillation. (Here, we have retained the same notation for the scaled plastic strain rate and stress as for the unscaled ones.) The unstable fixed point is also shown. Starting from any initial value around the unstable focus, trajectories spiral out converging onto the limit cycle. In Fig. 7, we have identified different regions of the phase space with different regions of the slow manifold, S_1 and S_2. We first note that there is a considerable similarity between Fig. 7 and the schematic representation of the relaxational oscillation obtained using the negative SRS shown in Fig. 1. Note also that in contrast to the artificial flat parts $B'C'$ and $C'D'$ of Fig. 1, the equivalent parts in Fig. 7 have a finite negative slope. Last, as in experiments, the strain rate jump from B to C is over two orders of magnitude.

Here, we set up a correspondence between the dynamics in the phase space (Fig. 7) and the slow manifold (Figs. 4 and 5). From our earlier discussion, we know that when the trajectory is on S_2, x is constant and small in magnitude. Consequently, according to Eq. (9), ϕ should increase linearly and hence this corresponds the rising branch AB in Fig. 7. Further, noting that $\dot{x} \sim 0$ for the entire interval of time spent by the trajectory on S_2 (see Fig. 4), the branch AB of Fig. 7 corresponds to the pinned state of dislocations. For this branch, one can easily see that the (mean) value of $\mathcal{S} \sim 3.5$ using Eq. (14). Further, as we move up on this branch towards B (Fig. 4), the value of δ approaches zero, and ϕ reaches its maximum value. Once δ becomes positive, the trajectory leaves S_2, and thus, the strain rate jump from B to C in Fig. 7, and corresponds to the trajectory jumping from

S_2 to S_1 in Figs. 4 and 5. Note that the slope $\partial\phi/\partial\dot{\epsilon}_p$ for this portion of the orbit is quite small and negative unlike the zero value for the equivalent part in Fig. 1. Further, we know from Fig. 4, once the trajectory reaches S_1, the value of x decreases rapidly resulting in the decrease of $\dot{\epsilon}_p$. Thus, the region CD in Fig. 7 corresponds to the movement of the trajectory on S_1 (in Fig. 4 for which $\delta>0$). For this branch, one can quickly check that the strain rate sensitivity $\mathcal{S}$ is positive, having a mean value (~ 1.5) which is a factor of 2 less than that for the branch AB, implying that the nature of dissipation is quite different from that operating on AB. This is consistent with known facts about the two branches as mentioned in the Introduction. Combining this with the fact that $\dot{x}$ is decreasing, the branch CD in Fig. 7 mimics the equivalent branch $C'D'$ in Fig. 1, which is identified with the slowing down of the mobile dislocations without solute atmosphere.

We recall that the stress drop duration has contributions from two fast processes, namely, dislocation multiplication and its subsequent immobilization. But, these two time scales could not be separated in the stress-strain curve. However, in the present phase plot representation (Fig. 7), we see that the fast multiplication of dislocations correspond to BC and that of immobilization to CD. This correspondence has been possible due to the mapping of the relevant time scales in the dynamics of the dislocations obtained from the analysis of the slow manifold to the various regions in the phase plot thereby allowing us to identify the individual contributions. (Note also that in Fig. 7, we have plotted points of the trajectory at equal intervals of time which shows that the time interval corresponding to BD is small.) From Figs. 4 and 5, we see that as the trajectory descends on the S_1 part of the slow manifold and gets close to S_2, it leaves S_1, since $\partial g/\partial x$ becomes positive ($x\sim 50$). Further, the strain rate sensitivity parameter $\mathcal{S}$ changes sign at D. For the corresponding DA part in Fig. 7, the slope is small and negative as for the part BC. Noting that B and D are the points at which $\mathcal{S}$ turns negative, and noting that the fixed point is unstable, *the so called ''unstable branch'' of the SRS, not accessible to the dynamics, can be inferred by drawing a (dotted) line connecting the maximum and the minimum of the stress and passing it through the unstable fixed point* (Fig. 7).

We will now attempt to use the results of our analysis of time scales in different regions of the slow manifold to obtain the dependence of $\dot{\epsilon}_p$ as a function of ϕ. The equation for $\dot{\epsilon}_p$ is

$$\frac{d\dot{\epsilon}_p}{dt} = xm\phi^{m-1}\dot{\phi} + \phi^m\dot{x}, \tag{15}$$

which on using Eqs. (6) and (9) gives

$$\frac{d\dot{\epsilon}_p}{d\phi} = \frac{\dot{\epsilon}_p\left(\frac{mde}{\phi}+\delta\right) - \dot{\epsilon}_p^2\left(\frac{md}{\phi}+\frac{b}{\phi^m}\right) + y\phi^m}{d(e-\dot{\epsilon}_p)}. \tag{16}$$

Here we note that in the slow manifold description, all slow variables appear as parameters. However, since SRS describes the dependence of the slow variable ϕ as a function of the (derived) fast variable $\dot{\epsilon}_p$, we will consider the other two variables y or δ or both as parameters. Numerical solution of Eq. (16) has been attempted using y and δ as parameters. Good numerical approximation is obtained by noting that y and hence δ is periodic. Thus, any reasonable approximation for the periodicity of y, for example, sine function with a proper amplitude and phase, gives a good fit with the phase plot. However, our interest here is to obtain approximate expressions for $\dot{\epsilon}_p(\phi)$ on different branches. For this reason, we will use typical values of δ and y for the interval under question. From Sec. IV, the trajectory has different dynamics in different regions of the slow manifold. These are (1) on S_2 where $\dot{x}$ is nearly zero for the entire time spent by the trajectory on S_2, (2) just outside S_2 where $\dot{x}\sim x\delta$, (3) on S_1 where $x\sim\delta/b_0$ for $\dot{\epsilon}_p>e$, and (4) when the trajectory jumps from S_1 to S_2. Approximate solutions obtained for these cases are shown in the phase plot by solid lines. Details are given in the Appendix. It is clear that these solid lines reproduce the general features of the phase plot quite well. We stress here that these lines correspond to the simplest approximation.

The above analysis refers to a fixed value of e. As a function of e, we find that the magnitude of the stress drops, increases initially, and then decreases. This feature is a direct result of the existence of back-to-back Hopf bifurcations in the model. On the other hand, experimentally one sees only a decreasing trend. While the decreasing trend is consistent, the increasing trend seen in the model for low strain values can be traced to the effect of another crucial parameter in the model, namely, b_0. We recall that this parameter corresponds to the remobilization of immobile dislocations. For the value of b_0 used in the present calculation, the bifurcation from the steady state is a mildly subcritical Hopf bifurcation, i.e., across the transition the amplitude of the stress change is abrupt but the magnitude is small. However, for smaller values of b_0, this jump can be made sufficiently large in which case the amplitude of the stress drops can be made to decrease with e right from the onset of the PLC effect.

VI. DISCUSSION AND CONCLUSIONS

The study of the relaxation oscillations in the model was motivated by the need to explain the apparent inconsistency between the time scales observed in experimental stress-time series and those that could be argued on the basis of the negative SRS feature commonly used in the literature. The study of relaxation oscillations using the geometry of the slow manifold has helped us to identify different time scales operating in different regions of the phase space, apart from showing that the nature of the relaxation in the model is due to the atypical bent geometry of the slow manifold. This geometry is very different from the standard S-shaped manifold and hence the relaxation oscillations seen here differ qualitatively from those seen in systems with S-shaped slow manifold. Some comparative comments between these two types of manifolds may be in order here. As in the S-shaped manifold, there are two attracting branches in our case also, namely, S_1 and S_2. The dynamics on S_2 is slow as it is controlled by the slow variables y and ϕ. On the other hand, on S_1, the time dependence of the trajectory is largely con-

trolled by the fast variable x. In this sense, the dynamics on S_2 is slow and that on S_1 is fast. Though there are two fast jumps as in the S-shaped manifold, in our case, there is no equivalent unstable part of the slow manifold which causes these jumps.

The analysis of the time scales controlling the relaxation oscillations has been directly used to reconstruct the relaxation oscillation in the ϕ-$\dot{\epsilon}_p$ plane which bears a strong resemblance to the relaxation oscillations resulting from the assumed form of the negative SRS. The information on different time scales operating in different regions of the slow manifold has been used to calculate the dependence of ϕ on $\dot{\epsilon}_p$ for the two dissipative branches and the associated strain rate jumps between them. This has helped to identify the various regions of the slow manifold with the stick state and the slip state of dislocations. It has also helped us to clarify the inconsistency in the time scales of the dynamics. Further, several important features of the SRS derived from the model compare well with those reported in the literature. In particular, we note that the slope of the first dissipative branch AB is larger than that of the second branch CD (Fig. 7). Further, we recall that $-\delta = -\phi^m + y + a$ which is positive for AB, gradually approaches zero as B is reached followed by strain rate jump. Similarly, for the branch CD, δ approaches zero as we approach D followed by a jump in the strain rate. Thus, vanishing of δ is indicative of strain rate jumps just as the strain rate sensitivity also vanishes. Noting that y is the immobile dislocation density, it is tempting to interpret δ as being related to some kind of effective stress. (Recall that the effective stress is $\sigma^* = \sigma_a - HN_{im}^{1/2}$, where H is the work hardening coefficient.) Thus, the points at which strain rate jumps occur correspond to points at which the effective stress vanishes which is very much like the classical explanation. Since the definition of strain rate sensitivity assumes strain as a state variable which is not true, δ may be an effective alternate parameter for defining strain rate sensitivity. Thus, it is nice to see that we can attribute a physical meaning to this parameter.

The analysis has also helped us to provide a dynamical interpretation of the negative SRS. The analysis also shows that the large jumps in the strain rate across the stable branches are due to the relaxational nature of the dynamics which in turn is a result of the bent nature of the slow manifold and the fact that the bifurcation is of the Hopf type. Using this, we have inferred the existence of the unstable branch as containing the two points, B and D, where strain rate jumps (where δ and S are zero) and the unstable fixed point is located. In this sense, Hopf bifurcation is at the root of the ''negative'' SRS. Similar features of SRS were found to operate in a model designed to mimic stick-slip dynamics of tectonic faults [35]. There are other studies on stick-slip dynamics, both experimental [36] and theoretical [37], which support the view that Hopf bifurcation was found to be responsible for the instability. Thus, it is likely that Hopf bifurcation is relevant to situations where stick-slip dynamics operates and wherever one measures the two stable branches and the jumps across the branches [38].

The relaxation oscillations in the model are reminiscent of the *canard* type of oscillations in multiple type scale dynamical systems [39,40]. The latter type of oscillations result from ''sticking'' of the trajectory to the repelling part of the S-shaped slow manifold before jumping to the attracting pleat of the slow manifold. In our case, although these oscillations have a similarity with canard type of solutions, the repelling part of slow manifold does not exist. Instead, the trajectories stick to the unstable part of the phase space where the dynamics is accelerated once the trajectory moves well into this region. This aspect coupled to the fact that there is no inherent constraint on the manifold structure leads to oscillations of all sizes. It is clear that such oscillations result from the trajectory sticking to the direction of the S_2 plane and moving into the unstable part of the phase space by varying amounts each time the trajectory visits S_2. These jumps translate into stress drops of varying sizes which are generally seen in experimental time series (Fig. 2). This also means that $\dot{\epsilon}_p - \phi$ is not a simple limit cycle, and the simplistic approach of inferring the ''negative'' SRS should be given up. The present analysis stresses the importance of using sound dynamical tools such as the slow manifold as the basis for studying more complex oscillations rather than phenomenological concepts such as the negative SRS.

APPENDIX

Here we obtain approximate analytical expressions for $\dot{\epsilon}_p(\phi)$ for different regions of the ϕ-$\dot{\epsilon}_p$ phase plot (Fig. 7) using the knowledge of time scales obtained from the analysis of relaxation oscillations. For the numerical evaluation, the values of control parameters have been chosen as $e = 200$, $m = 1.2$, $b_0 = 0.002$, and $d = 0.0001$.

Region AB: When the trajectory is on S_2, $\dot{x} \sim 0$, for the entire interval of time. Using $x = -y/\delta$ in Eq. (15), we get

$$\frac{d\dot{\epsilon}_p}{d\phi} = -\frac{\phi^{m-1} m y}{\delta}. \tag{A1}$$

Noting that $\delta = \phi^m - y - a$, this equation can be integrated thereby reducing the number of parameters to one, namely, y. Integrating, we get

$$\dot{\epsilon}_p = -y \ln\left(\frac{\phi^m - (y+a)}{\phi^m(0) - (y+a)}\right) + \dot{\epsilon}_p(0), \tag{A2}$$

where $\dot{\epsilon}_p(0)$ and $\phi(0)$ refer to their respective values as the trajectory enters S_2. In Fig. 7, we have used $\dot{\epsilon}_p(0) = 4.7$, $\phi(0) = 2.2$, and $y = 6.15$.

Region BC: This region corresponds to the jump from S_2 to S_1. This happens when the trajectory is just outside S_2. For this region, ϕ is near ϕ_{max}, and since $x \sim (y/b_0)^{1/2}$, the evolution of x is well described by $\dot{x} \sim x\delta$, implying that the time of evolution is very short. Thus, we can regard the evolution of ϕ as being mainly determined by that of x. (This region also corresponds to $\delta > 0$ and small ~ 0.2.) Thus, we use $\phi = \phi_{max}$ on the right-hand side of Eq. (9). Then,

$$\frac{d\phi}{dt} = d(e - \phi_{max}^m x_{s_2} e^{\delta t}), \tag{A3}$$

where x_{s_2} is the value of x at the time of leaving S_2. Integrating this equation with initial conditions at $t=0$, $\phi=\phi(0)=\phi_{max}$, we get

$$e^{\delta t}=\frac{te\delta}{x_{s_2}\phi_{max}^m}-\frac{(\phi(t)-\phi_{max})\delta}{x_{s_2}\phi_{max}^m d}+1. \tag{A4}$$

Clearly, the first term is small since the time span of evolution that we are interested in is also $\sim\delta$. Now consider Eq. (15). Using $\dot{x}\sim x\delta$, we get

$$\frac{d\dot{\epsilon}_p}{dt}=\dot{\epsilon}_p\left(\frac{med}{\phi_{max}}+\delta\right)-\frac{m\dot{\epsilon}_p^2 d}{\phi_{max}}. \tag{A5}$$

Since $med/\phi_{max}\ll\delta$, we drop the first term. Integrating the above equation with the initial value $\dot{\epsilon}_p(0)=e$, leads to

$$\dot{\epsilon}_p=\frac{\phi_{max}e[\phi_{max}-\phi(t)]\delta}{md^2\phi_{max}^m x_{s_2}(\phi_{max}\delta/md-e)-[\phi(t)-\phi_{max}]emd}. \tag{A6}$$

In Fig. 7, we have used the values $\delta=0.021$, $\phi_{max}=4.98$, and $x_{s_2}=1.7$.

Region CD: Consider the trajectory on S_1 with $x\sim\delta/b_0$ and $\dot{\epsilon}_p\gg e$. Then, Eq. (16) reads,

$$\frac{d\dot{\epsilon}_p}{d\phi}=-\frac{\dot{\epsilon}_p\left(\frac{med}{\phi}+\delta\right)-\dot{\epsilon}_p^2\left(\frac{md}{\phi}+\frac{b_0}{\phi^m}\right)+y\phi^m}{d\dot{\epsilon}_p\left(1-\frac{e}{\dot{\epsilon}_p}\right)}. \tag{A7}$$

Since $e/\dot{\epsilon}_p<1.0$, we expand the denominator and retain terms upto $\dot{\epsilon}_p^{-1}$. We note here that on S_1, x is rapidly decreasing and therefore, using slow manifold values is not a good approximation. Even so, as a simplest approximation we use $x\sim\delta/b_0$. Then, we get

$$\frac{d\dot{\epsilon}_p}{d\phi}=-\frac{me^2b_0}{\phi^{m+1}\delta}-\frac{eb_0^2y}{\phi^m d\delta^2}+\frac{m\phi^{m-1}\delta}{b_0}-\frac{b_0y}{d\delta}. \tag{A8}$$

In this equation, both y and δ appear as parameters whose values are chosen appropriate to this region. Integrating the above equation with the initial values of $\phi(0)$ and $\dot{\epsilon}_p(0)$, we get

$$\begin{aligned}\dot{\epsilon}_p=&\frac{eb_0^2y}{(m-1)d\delta^2}[\phi^{1-m}-\phi^{1-m}(0)]\\&+\frac{e^2b_0}{\delta}[\phi^{-m}-\phi^{-m}(0)]+\frac{\delta}{b_0}[\phi^m-\phi^m(0)]\\&-\frac{b_0y}{d\delta}[\phi-\phi(0)]+\dot{\epsilon}_p(0).\end{aligned} \tag{A9}$$

In Fig. 7, we have used the values of $\delta=3.57$, $y=1.0$ with $\phi(0)=4.3$ and $\dot{\epsilon}_p(0)=7460.0$.

Region DA: This region again corresponds to the trajectory descending on S_1 but $\dot{\epsilon}_p<e$. Then, Eq.(16) can be written in the form

$$\frac{d\dot{\epsilon}_p}{d\phi}=-\frac{\dot{\epsilon}_p\left(\frac{med}{\phi}+\delta\right)-\dot{\epsilon}_p^2\left(\frac{md}{\phi}+\frac{b_0}{\phi^m}\right)+y\phi^m}{ed\left(1-\frac{\dot{\epsilon}_p}{e}\right)}. \tag{A10}$$

In this region, the value of ϕ is slowly varying with its value near the minimum for which $\delta\sim-0.15$. Since ϕ is near ϕ_{min}, we use $\phi=\phi_{min}$ and regard the variation as largely arising due to the changes in $\dot{\epsilon}_p$. Using $(1-\dot{\epsilon}_p/e)^{-1}\approx(1+\dot{\epsilon}_p/e)$, we have

$$\frac{d\dot{\epsilon}_p}{d\phi}=-(A_1\dot{\epsilon}_p+B_1\dot{\epsilon}_p^2-C_1\dot{\epsilon}_p^3), \tag{A11}$$

where $A_1=(m/\phi_{min})-(|\delta|/ed)$, and $B_1=-(|\delta|/e^2d)-(b_0/e\phi_{min}^m d)$ and $C_1=(m/\phi_{min}e^2)+(b_0/e^2d\phi_{min}^m)$. Since $C_1\ll A_1$ and B_1, we drop the last term. Integrating the above equation with the initial conditions, $\phi(0)=\phi_{min}$ and $\dot{\epsilon}_p=e$, we get

$$\dot{\epsilon}_p=\frac{eA_1e^{A_1(\phi-\phi_{min})}}{A_1+eB_1(1-e^{A_1(\phi-\phi_{min})})}. \tag{A12}$$

In Fig. 7, we have used $\phi_{min}=1.55$.

[1] F. Le Chatelier, Re. de Metallurgie **6**, 914 (1909); A. Portevin and F. Le Chatelier, C. R. Acad. Sci. **176**, 507 (1923).

[2] A. H. Cottrell, Philos. Mag. **44**, 829 (1953).

[3] B. J. Brindley and P. J. Worthington, Metall. Rev. **145**, 101 (1970).

[4] Scr. Metall. Mater. **29**, 8 (1993), special issue on view point set No.21, edited by L. P. Kubin, Y. Estrin, and E. C. Aifantis.

[5] P. G. McCormick, Acta Metall. **20**, 351 (1972).

[6] A. van den Beukel, Phys. Status Solidi A **30**, 197 (1975).

[7] L. P. Kubin and Y. Estrin, Acta Metall. **33**, 397 (1985).

[8] G. Ananthakrishna and M. C. Valsakumar, J. Phys. D **15**, L171 (1982). The basic model was formulated in G. Ananthakrishna and D. Sahoo, *ibid.* **14**, 2081 (1981).

[9] *Non Linear Phenomena in Materials Science*, Solid State Phenomena Vols. 3 and 4, edited by L. P. Kubin and G. Martin (Trans Tech, Switzerland, 1988), and references therein.

[10] *Non Linear Phenomena in Materials Science II*, edited by G. Martin and L. P. Kubin (Trans Tech, Zurich, 1992), and references therein.

[11] *Non Linear Phenomena in Materials Science III*, edited by G.

Ananthakrishna, L. P. Kubin, and G. Martin (Scitec, Zurich, 1995), and references therein.
[12] G. Ananthakrishna, C. Fressengeas, M. Grosbras, J. Vergnol, C. Engelke, J. Plessing, H. Neuhäuser, E. Bouchaud, J. Planes, and L. P. Kubin, Scr. Metall. Mater. **32**, 1731 (1995).
[13] G. Ananthakrishna and S. J. Noronha, in *Nonlinear Phenomena in Materials Science III* (Ref. [11]).
[14] S. J. Noronha, G. Ananthakrishna, L. Quaouire, C. Fressengeas, and L. P. Kubin, Int. J. Bifurcation Chaos Appl. Sci. Eng. **7**, 2577 (1997).
[15] S. J. Noronha, G. Ananthakrishna, L. Quaouire, and C. Fressengeas, Pramana, J. Phys. **48**, 705 (1997).
[16] G. Ananthakrishna, Scr. Metall. Mater. **29**, 1183 (1993).
[17] M. Bekele and G. Ananthakrishna, Phys. Rev. E **56**, 6917 (1997).
[18] M. Bekele and G. Ananthakrishna, Int. J. Bifurcation Chaos Appl. Sci. Eng. **8**, 141 (1998).
[19] D. Maugis, J. Mater. Sci. **20**, 3041 (1985).
[20] *Physics of Sliding Friction*, Vol. 311 of *NATO Advanced Study Institute, Series E: Applied Sciences*, edited by B. N. J. Pearson and E. Tossatti (Kluwer Academic Publishers, Dordrecht, 1996).
[21] A. Rosen and S. R. Bodner, J. Mech. Phys. Solids **15**, 47 (1967).
[22] L. P. Kubin and Y. Estrin, J. Phys. (France) **47**, 497 (1986).
[23] P. Penning, Acta Metall. **20**, 1169 (1972).
[24] V. Jeanclaude and C. Fressengeas, C. R. Acad. Sci., Ser. II: Mec., Phys., Chim., Sci. Terre Univers **316**, 816 (1993).
[25] M. A. Lebyodkin, Y. Brechet, Y. Estrin, and L. P. Kubin, Phys. Rev. Lett. **74**, 4758 (1995).
[26] H. Neuhäuser, in *Dislocations in Solids*, edited by F. R. N. Nabarro (North-Holland, Amsterdam, 1993).
[27] A. Arneodo, F. Argoul, J. Elezgaray, and P. Richetti, Physica D **62**, 134 (1993).
[28] M. T. M. Koper, P. Gaspard, and J. H. Sluyters, J. Chem. Phys. **97**, 8250 (1992).
[29] D. Barkley, J. Chem. Phys. **89**, 5547 (1988).
[30] M. J. B. Hauser and L. F. Olsen, J. Chem. Soc., Faraday Trans. **92**, 2857 (1996).
[31] B. Deng, Int. J. Bifurcation Chaos Appl. Sci. Eng. **4**, 823 (1994).
[32] S. Rajesh and G. Ananthakrishna, Physica D (to be published).
[33] O. E. Rössler, Z. Naturforsch. A **31A**, 259 (1976).
[34] L. P. Kubin and Y. Estrin, Scr. Metall. Mater. **23**, 815 (1989).
[35] G. Ananthakrishna and H. Ramachandran, in *Nonlinearity and Breakdown in Soft Condensed Matter*, Vol. 437 of *Lecture Notes in Physics*, edited by K. K. Bardhan, B. K. Chakrabarti, and A. Hansen (Springer-Verlag, Heidelberg, 1994).
[36] F. Heslot, T. Baumberger, B. Perrin, B. Caroli, and C. Caroli, Phys. Rev. E **49**, 4973 (1994).
[37] See C. Caroli and P. Noziers, in *Physics of Sliding Friction* (Ref. [20]).
[38] G. Ananthakrishna, in *Nonlinearities in Complex Systems*, edited by S. Puri and S. Dattagupta (Narosa Publishing House, New Delhi, 1997).
[39] A. Milik, P. Szmolyan, H. Löffelmann, and E. Gröller, Int. J. Bifurcation Chaos Appl. Sci. Eng. **8**, 505 (1998).
[40] W. Eckhaus, Lect. Notes Math. **905**, 432 (1983).